Quinolinoacridine as High Efficiency Building Unit in Single-Layer Phosphorescent Organic Light-Emitting Diodes

Clement Brouillac, Fabien Lucas, Denis Ari, Denis Tondelier, Jonathan Meot, Marc Malvaux, Cyril Jadaud, Christophe Lebreton, Joëlle Rault-Berthelot, Cassandre Quinton, et al.

ADVANCED ELECTRONIC MATERIALS Open Access
www.advelectronicmat.de

Quinolinoacridine as High Efficiency Building Unit in Single-Layer Phosphorescent Organic Light-Emitting Diodes

*Clément Brouillac, Fabien Lucas, Denis Ari, Denis Tondelier, Jonathan Meot, Marc Malvaux, Cyril Jadaud, Christophe Lebreton, Joëlle Rault-Berthelot, Cassandre Quinton, Emmanuel Jacques, and Cyril Poriel**

Dedicated to Joëlle Rault-Berthelot on the occasion of her retirement

The performances of simplified single-layer phosphorescent organic light-emitting diodes (SL-PhOLEDs) have significantly increased and they now appear to be a promising alternative to multi-layer PhOLEDs. The blue and white emissions, far more challenging than all the other colours, are still particularly desired. Herein, a high efficiency host material for blue emitting SL-PhOLED using the blue emitter FIr6 is reported, which is particularly interesting as it displays an emission at shorter wavelengths than the well-known FIrpic emitter, almost exclusively reported in the SL-PhOLEDs literature. The host material investigated herein is constructed on the electron-rich quinolinoacridine and displays when incorporated in FIr6-based SL-PhOLEDs, an external quantum efficiency (EQE)〉10% and a low Von of 3.1 V. This is the first work passing an EQE of 10% with FIr6 as an emitter. This host also reaches a very high EQE of 19% when used with the green emitter Ir(ppy)2acac, this performance being among the highest recorded for green SL-PhOLEDs. Finally, as white SL-PhOLEDs involve blue emitting SL-PhOLEDs, this host is also used with a combination of blue and yellow emitters. An extremely high EQE of 24% is reached with CIE coordinates of (0.40;0.48). These findings show the real potential of the quinolinoacridine fragment to reach high performance multi-colour SL-PhOLEDs.

1. Introduction

Blue emission is a central concept in the field of optoelectronics and particularly in organic light emitting diode (OLED) technology.[1–5] For the last twenty years, many research groups worldwide have developed various strategies to reach efficient and stable blue emission for the three generations of OLEDs, i.e fluorescent, phosphorescent and Thermally Activated Delayed Fluorescent (TADF) OLEDs.[1,4,6–9] This is particularly challenging for the new generations of simplified Single-Layer Phosphorescent OLEDs (SL-PhOLEDs), which have made great progress in the recent years.[10] These simplified devices do not possess any functional layers, which usually insure in a "classical" OLED (with a multi-layer stack) the injection, the transport and the recombination of the charges within the Emissive layer (EML). Consequently, all these abilities should be gathered in the EML itself (organic host material and organometallic phosphorescent emitter). The difficulty to efficiently host blue phosphorescent emitters is notably due to their high E_T (above 2.6 eV) and their large HOMO/LUMO gap (above 3 eV). The most popular blue phosphor used in the field of PhOLEDs is the bis[2-(4,6-difluorophenyl)pyridinato-C,^{2}N](picolinato)iridium(III) commonly abbreviated FIrpic.[11] However, FIrpic displays an E_T of 2.67 eV (in 2-MeTHF at room temperature[12]) and a broad emission shifting it into the sky blue or greenish-blue region of the chromatic diagram (λ_{max} = 465 and 497 nm in

C. Brouillac, D. Ari, J. Rault-Berthelot, C. Quinton, C. Poriel
Univ Rennes
CNRS
ISCR-UMR CNRS 6226
Rennes F-35000, France
E-mail: cyril.poriel@univ-rennes1.fr

The ORCID identification number(s) for the author(s) of this article can be found under https://doi.org/10.1002/aelm.202300582

DOI: 10.1002/aelm.202300582

F. Lucas, D. Tondelier, J. Meot, M. Malvaux, C. Jadaud
LPICM
CNRS
Ecole Polytechnique
IPParis
Palaiseau 91128, France

C. Lebreton, E. Jacques
Univ Rennes
CNRS
IETR-UMR CNRS 6164
Rennes F-35000, France

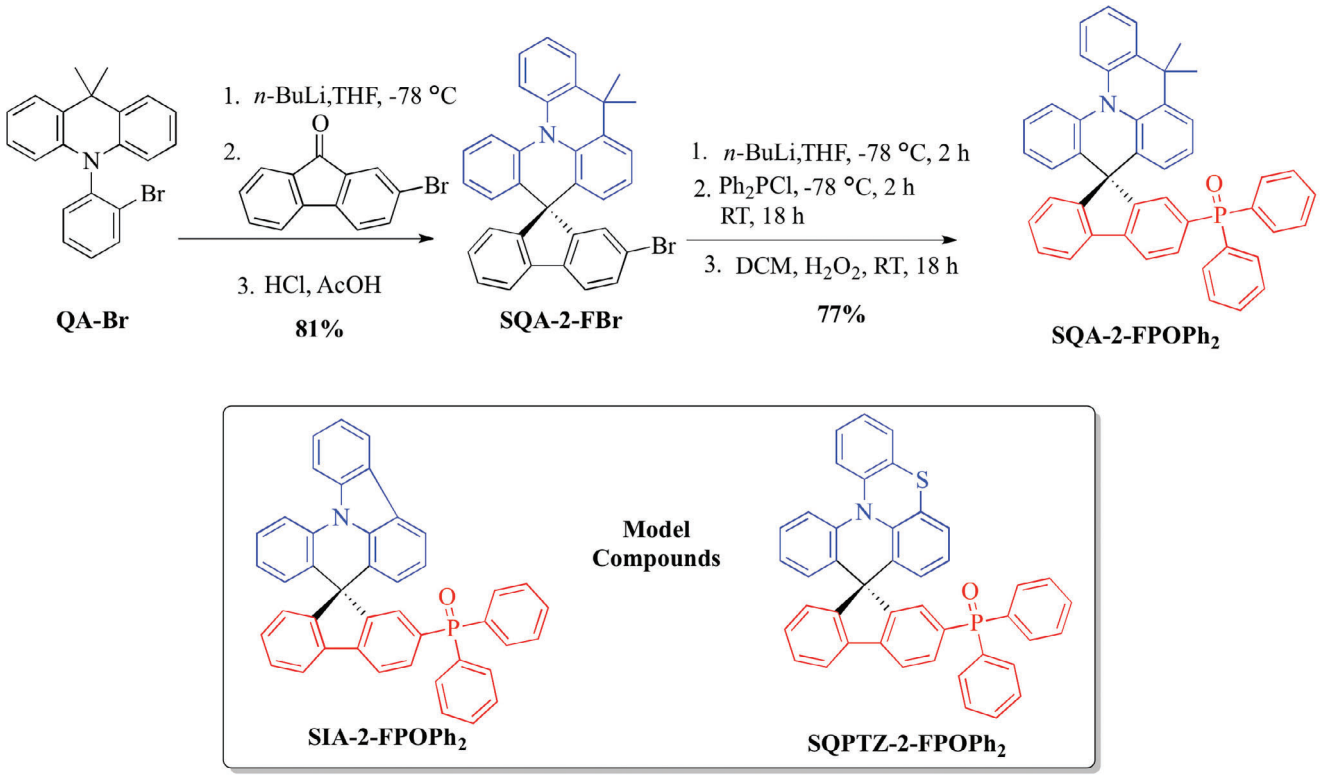

Scheme 1. Synthesis of **SQA-2-FPOPh$_2$** and model compounds **SIA-2-FPOPh$_2$** and **SQPTZ-2-FPOPh$_2$**.

2-MeTHF, CIE coordinates: 0.15; 0.37).[12] Its HOMO/LUMO energy levels are −5.55/−2.52 eV (obtained from electrochemical studies in CH_2Cl_2[12]), giving a gap of 3.03 eV. In addition to its greenish-blue emission, the main drawback of this phosphor is its instability when incorporated in an OLED. Indeed, FIrpic possesses datively bound nitrogen picolinate ligands, and it has been shown that this complex degrades through the loss of these ancillary ligands.[13–15] Bis(2,4-difluorophenylpyridinato)-tetrakis(1-pyrazolyl)borate iridium(III), FIr6,[16] displays a higher E_T (2.72 eV measured in 2-MeTHF at room temperature[12]) and bluer CIE coordinates (0.15;0.30)[12] than FIrpic. It also possesses an extended HOMO (−5.66 eV)/LUMO (−2.32 eV) gap (3.34 vs. 3.03 eV for FIrpic). Compared to FIrpic, its phosphorescence is therefore shifted to lower wavelengths (λ_{max} = 456 and 486 nm in 2-MeTHF[12]). However, FIr6 has been barely studied to date, with only one example in SL-PhOLED.[12] Several examples nevertheless exist in multi-layer devices.[17,18] The difficulty to host such a type of blue phosphor is surely at the origin of its absence. Thus, in blue SL-PhOLEDs, almost all examples reported to date use the sky-blue emitter FIrpic.[19–23]

In this SL-PhOLED technology, the molecular design of the material hosting the phosphor in the EML has been the driving force of the field as it has a strong impact on the device performance.[10] In this work, we report an efficient host material for FIr6-based SL-PhOLEDs, namely spiroquinolinoacridine-2-bis(diphenylphosphine oxide)-fluorene (**SQA-2-FPOPh$_2$**) constructed on a barely studied electron-rich 5,5-dimethyl-5,9-dihydroquinolino[3,2,1-d]acridine (QA) fragment.[24,25] Thanks to the association with the well-known electron-deficient 2-bis(diphenylphosphineoxide)-fluorene, the potential of this molecular fragment in blue emitting SL-PhOLEDs is evidenced. Used as host, we report for the first time in FIr6-based SL-PhOLED, an External Quantum Efficiency (EQE) above 10% and a low threshold voltage (V_{on}) of 3.1 V. Thanks to a comparative study with structurally related hosts (one is the most efficient host reported to date for green SL-PhOLED, namely **SQPTZ-2-FPOPh$_2$**[26]), we show the influence of the photophysical (radiative deactivation), morphological (AFM) and charge transport (charge carrier mobilities) properties on the performances. In green emitting SL-PhOLEDs, **SQA-2-FPOPh$_2$** also appears to be highly efficient with an EQE above 19%, in the same range than the best reported to date.[26] Finally, as the development of white SL-PhOLEDs involves blue emitting SL-PhOLEDs, this host was also used in a SL-PhOLED using a blue and a yellow emitter. An extremely high EQE of 24% was reached with CIE coordinates of (0.40;0.48). These performances show the potential of quinolinoacridine fragment to reach high performance single-layer devices with various phosphorescent emitters.

2. Results and Discussion

As reducing the number of steps in the synthetic approach is nowadays a mandatory step to decrease the environmental footprint of electronic devices, **SQA-2-FPOPh$_2$** was synthesized via a short and efficient high yielded approach (62% over the whole sequence), which allows a gram-scale preparation and purification (**Scheme 1**). The sequence involves first the coupling of 10-(2-bromophenyl)−9,9-dimethyl-9,10-dihydroacridine

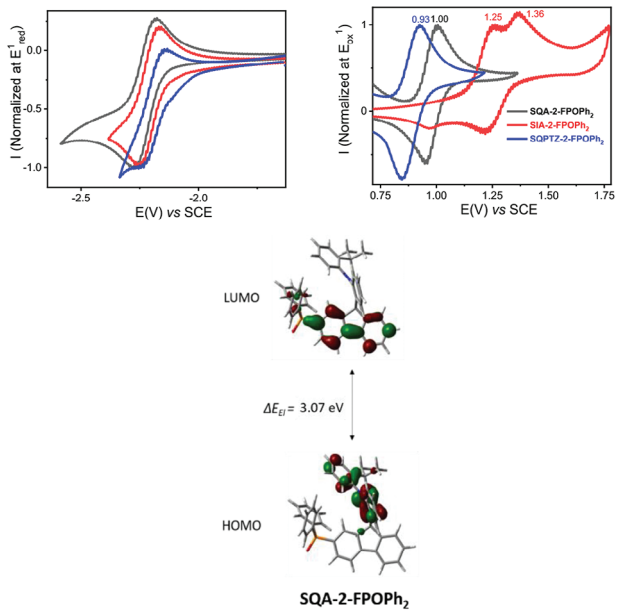

Figure 1. (Top) Cyclic voltammetry's recorded on Pt working electrode (left, DMF + Bu_4NPF_6 0.1 M, sweep-rate 100 mV s^{-1}) and in oxidation (right, CH_2Cl_2 + Bu_4NPF_6 0.2 M, sweep-rate 100 mV s^{-1}) of **SQA-2-FPOPh$_2$** (black lines), **SIA-2-FPOPh$_2$** (red lines) and **SQPTZ-2-FPOPh$_2$** (blue lines). (Bottom) Representation of HOMO/LUMO calculated by DFT for **SQA-2-FPOPh$_2$** (B3LYP/6-311+G(d,p)).

QA-Br with 2-bromofluorenone (*n*-BuLi) to form, after acidification, the **SQA-2-FBr** platform. Diphenylphosphine oxide unit is then attached by nucleophilic addition of the corresponding lithiated intermediate to chlorodiphenylphosphine and a final oxidation step with H_2O_2.

In order to evidence the impact of the QA fragment in the high performances obtained in **SL-PhOLEDs** (see below), two structurally related model compounds have also been investigated, namely spiroquinolinophenothiazine-2-fluorene(diphenylphosphine oxide) **SQPTZ-2-FPOPh$_2$** and spiroindoloacridine-2-(diphenylphosphine oxide)-fluorene **SIA-2-FPOPh$_2$** (**Scheme** 1). In these model compounds, the QA fragment has been replaced with another bridged phenylacridine-based fragment: either quinolinophenothiazine (sulfur bridge) in **SQPTZ-2-FPOPh$_2$** or indoloacridine (direct carbon–carbon bond coupling) in **SIA-2-FPOPh$_2$**. The quinolinophenothiazine fragment (QPTZ)[27–31] and the indoloacridine fragment (IA)[27,32–34] are both known to provide high efficiency host materials for PhOLEDs and fluorescent emitters. Particularly, **SQPTZ-2-FPOPh$_2$** is a known compound, very recently reported in literature, which possesses the highest performance (EQE of 22.7%) ever reported for a green-emitting SL-PhOLED.[35] These two model compounds have been synthesized following a similar approach as that described for **SQA-2-FPOPh$_2$** (see Supporting Information).

The determination of HOMO and LUMO energy levels has first been performed by cyclic voltammetry (CV) in CH_2Cl_2 for oxidation and in DMF for reduction; potentials are given versus a saturated calomel electrode (SCE), **Figure 1**. Interestingly, **SQA-2-FPOPh$_2$** displays first reversible oxidation and reduction waves, highlighting the stability of both radical cation and radical anion at the voltammetry time scale (Figure 1, top). The onset potentials were measured at 0.91 and −2.16 V respectively. The corresponding HOMO, imposed by the electron rich fragment, and LUMO, imposed by the electron-poor fragment, were then evaluated at −5.31 and −2.24 eV respectively. Molecular modelling shows that the HOMO and LUMO are almost exclusively spread out on the electron-rich and electron-poor units respectively, the *spiro* carbon insuring an efficient π-conjugation breaking between the two fragments. This is one of the key characteristics of the Donor-*spiro*-Acceptor molecular design and an important feature to keep a high triplet state energy (E_T), see below.

Compared to its quinolinophenothiazine analogue **SQPTZ-2-FPOPh$_2$**, one can note that the HOMO energy level of **SQA-2-FPOPh$_2$** is decreased (−5.20 vs. −5.31 eV) due to the different electron donating effects of the bridge (CMe_2 vs. S). The inverse trend is observed when compared to indoloacridine **SIA-2-FPOPh$_2$**, with a significant increase of the HOMO energy level (−5.53 vs. −5.31 eV). This highlights the different electron rich behaviour of the QA, IA and QPTZ fragments. Regarding the LUMO energy levels, the values obtained are deep, −2.24/−2.26 eV, and very similar as all centred on the same fragment, namely 2-bis(diphenylphosphineoxide)-fluorene.

The difference in terms of HOMO energy levels induces different electrochemical gaps (ΔE_{El}): 3.07 eV for **SQA-2-FPOPh$_2$**, 2.89 eV for **SQPTZ-2-FPOPh$_2$** and 3.27 eV for **SIA-2-FPOPh$_2$**. As the HOMO and LUMO are spatially separated thanks to the *spiro* carbon, this allows to gather in a single material i) HOMO/LUMO energy levels of the constituting building blocks, ii) a short π-conjugation pathway and iii) a high E_T (see below).

The UV–vis absorption and emission spectra of **SQA-2-FPOPh$_2$** (black line), **SIA-2-FPOPh$_2$** (red line), and **SQPTZ-2-FPOPh$_2$** (blue line) were recorded in cyclohexane at room temperature (**Figure 2**). The optical properties are summarized in **Table 1**. The three molecules show absorption up to 365 nm, which can be attributed to π–π* transitions. The TD-DFT calculations (**Figure 3**) indicate that the HOMO-LUMO transition is almost forbidden (with oscillator strengths of 0.001-0.002 for **SQPTZ-2-FPOPh$_2$** and **SQA-2-FPOPh$_2$** respectively). This is due to the *spiro* carbon, which allows for good spatial separation between the HOMO localized on the donor (QA or QPTZ) and the LUMO localized on the accepting fluorene core. In the case of **SIA-2-FPOPh$_2$**, a small band is present at 355 nm corresponding to the HOMO-LUMO transition, which has a higher oscillator strength (f = 0.009).

Additionally, The TD-DFT calculations show that the bands seen at 318 nm in the experiments are the consequence of the HOMO-1→LUMO transition between orbitals that are both localized on the fluorene part. This transition is detected at 303–307 nm for all three compounds and shows good agreement between the theoretical and experimental results. The bands at lower energy in the case of **SIA-2-FPOPh$_2$** are due to two transitions: HOMO→L+1 (localized on the indoloacridine part) and HOMO→L+2 (displaying a charge transfer character).

In emission spectroscopy, we note a gradual red shift of the maxima from **SIA-2-FPOPh$_2$** (356 nm) to **SQA-2-FPOPh$_2$** (384 nm), and to **SQPTZ-2-FPOPh$_2$** (420 nm). Thus, oppositely to their absorption spectra, **SQPTZ-2-FPOPh$_2$** and **SQA-2-FPOPh$_2$**

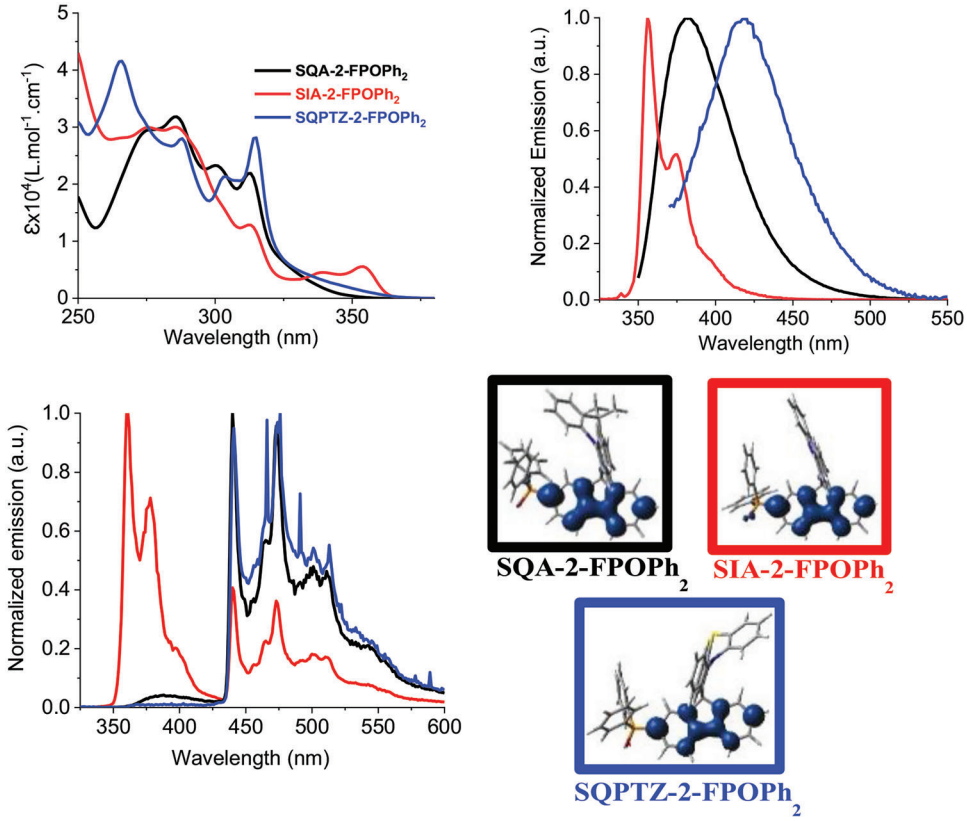

Figure 2. **SQA-2-FPOPh$_2$** (black lines), **SIA-2-FPOPh$_2$** (red lines) and **SQPTZ-2-FPOPh$_2$** (blue lines). UV–vis absorption spectra in cyclohexane (top-left). Emission spectra at room temperature in cyclohexane (λ_{exc} = 310 nm for **SQA-2-FPOPh$_2$** and **SIA-2-FPOPh$_2$**; λ_{exc} = 350 nm for **SQPTZ-2-FPOPh$_2$**, top-right). Emission spectra normalized at 77 K in 2-MeTHF (λ_{exc} = 310 nm, bottom-left). Triplet spin density distribution (TD-DFT, B3LYP/6-311+g(d,p), isovalue 0.004, bottom-right).

present different emission spectra, the spectrum of **SQPTZ-2-FPOPh$_2$** being significantly shifted by 36 nm (Figure 2, top right). Studying the evolution of the emission spectra as a function of the polarity of the solvent allows to go deeper into the polarity of the excited states. For **SQA-2-FPOPh$_2$**, a red shift of 92 nm between apolar cyclohexane (384 nm) and polar MeOH (476 nm) is measured, highlighting a strong photoinduced intramolecular charge transfer (ICT) (**Figure 4**, middle). The intensity of the ICT is then decreased in the case of **SIA-2-FPOPh$_2$** with a difference of 82 nm between cyclohexane (356 nm) and MeOH (438 nm), translating the weaker electron donating strength of IA versus QA (Figure 4-right). In addition, we note a different evolution of the spectra. Indeed, in **SIA-2-FPOPh$_2$**, the band becomes very large in polar EtOH and MeOH (ICT state) and thin and resolved in the other solvents (locally excited state). **SQA-2-FPOPh$_2$** does not present such a behaviour. The largest difference is observed for **SQPTZ-2-FPOPh$_2$** with a shift of 121 nm in accordance with the strong electron rich nature of the QPTZ fragment (Figure 4, left).

The differences ($\Delta\mu$) between the dipole moment at the ground state (μ) and at the first excited state ($\mu*$) have been evaluated using the Lippert-Mataga formalism. $\Delta\mu$ of 23.5, 16.5, and 14.4 D have been measured (the dipole moments at the ground state have been obtained by DFT calculations, 4.5, 4.9 and 4.1 D for **SQPTZ-2-FPOPh$_2$**, **SQA-2-FPOPh$_2$** and **SIA-2-FPOPh$_2$**, respectively, see Supporting Information). These $\Delta\mu$ data translate the different polarity of the three fluorophores at the excited state ($\mu*$ = 28.0, 21.4, and 18.5 D resp.). The significant red shift of the emission maxima (Figure 4) and the corresponding high $\Delta\mu$ observed for **SQPTZ-2-FPOPh$_2$** reveal an important photoinduced ICT. The decrease of $\Delta\mu$ from **SQA-2-FPOPh$_2$** and **SIA-2-FPOPh$_2$** is in accordance with a decrease of the photoinduced ICT. Thus, the polarity of excited states follows the strength of the electron-rich fragment QPTZ>QA>IA.

The E_T of the three compounds measured at 77 K in 2MeTHF (Figure 2, bottom left) is almost identical and very high: 2.81–2.82 eV. Indeed, the T_1 state is fully governed by the same fragment 2-fluorene(diphenylphosphineoxide) fragment. This is confirmed by the triplet spin density distribution (SDD) obtained by TD-DFT (b3lyp/6-311+g(d,p), Figure 2, bottom right), which shows for the three materials a triplet state density located on this fragment with no contribution of the donor unit. These values are very close to that of fluorene (2.93 eV),[36] with a decrease of ≈0.1 eV, which can be imputed to the presence of one phosphine oxide at C2 and to the interaction with the donor unit via spiro-conjugation. This feature has been previously observed with structurally related spiro compounds.[37] A very long lifetime of the emission at 77 K is measured for the three compounds, 4.3 s for **SQA-2-FPOPh$_2$**, 4.0 s for **SQPTZ-2-FPOPh$_2$** and 3.2 s for **SIA-2-FPOPh$_2$** in accordance with a phosphorescent

Table 1. Selected electronic and physical data of **SQA-2-FPOPh$_2$**, **SIA-2-FPOPh$_2$** and **SQPTZ-2-FPOPh$_2$**.

	SQPTZ-2-FPOPh$_2$ [n)]	**SQA-2-FPOPh$_2$**	**SIA-2-FPOPh$_2$**
$\lambda_{abs\ max}$ [nm][a)] ($\varepsilon \times 10^4$ [L mol^{-1} cm^{-1}])	315 (2.8); 303 (2.0); 288 (2.8); 266 (4.1)	286 (3.2); 300 (2.3); 313 (2.2)	286 (3.0), 313 (1.3); 354 (0.5)
$\lambda_{em\ fluo}$ [nm][a,b)]	420	384	356, 375
QY [a,b)]	<0.01	0.01	0.29
$\lambda_{em\ phospho}$ [nm][b,c)]	441	440	440
E_T (eV)[b–d)]	2.81	2.82	2.82
τ_p [s] (λ_{em} [nm])[b,c)]	3.97 (441)	4.30 (440)	3.22 (440)
E_{onset}^{ox} [*V* vs *SCE*][e,f)]	0.8	0.91	1.13
E_{onset}^{red} [*V* vs *SCE*][e,g)]	−2.09	−2.16	−2.14
$HOMO_{exp}$ (eV)[h)]	−5.20	−5.31	−5.53
$LUMO_{exp}$ (eV)[h)]	−2.31	−2.24	−2.26
$HOMO_{th}$ (eV)[i)]	−5.49	−5.46	−5.75
$LUMO_{th}$ (eV)[i)]	−1.76	−1.68	−1.69
ΔE_{el} (eV)[h,j)]	2.89	3.07	3.27
ΔE_{theo} (eV)[i,j)]	3.73	3.78	4.06
μ_h (cm^2/V.s)[k)]	5.10×10^{-8}	7.25×10^{-5}	1.45×10^{-2}
μ_e (cm^2/V.s)[k)]	1.10×10^{-4}	1.35×10^{-7}	8.53×10^{-8}
T_d (°C)[l)]	399	408	407
T_g (°C)[m)]	150	149	128

[a)] in cyclohexane at RT; [b)] λ_{exc} = 310 nm; [c)] in 2-MeTHF at 77 K; [d)] from first phosphorescence peak; [e)] versus SCE; [f)] in CH_2Cl_2; [g)] in DMF; [h)] from electrochemical data; [i)] from theoretical calculation; [j)] ΔE_{el} = |HOMO-LUMO|; [k)] determined from SCLC devices analysis; [l)] determined by TGA; [m)] determined by DSC (2nd heating); [n)] from Ref. [26].

emission. One can note that, at 77 K, the fluorescence contribution of the three compounds is drastically different. Indeed, in the case of **SIA-2-FPOPh$_2$**, the fluorescence contribution is far more intense than the phosphorescence one whereas for both **SQA-2-FPOPh$_2$** and **SQPTZ-2-FPOPh$_2$**, the fluorescence contribution is extremely weak. This can be correlated to the difference observed in terms of quantum yield. The fluorescence quantum yields of both **SQA-2-FPOPh$_2$** and **SQPTZ-2-FPOPh$_2$** are measured to be below 0.01 in solution in cyclohexane. This is expected in view of the very low oscillator strength arising from the spatial separation of the donor and the acceptor fragments, which promotes a vanishingly small transition dipole moment between the S_1 and S_0 states (see below). **SIA-2-FPOPh$_2$** displays a different behaviour with a quantum yield slightly increased to ≈0.29, due to the higher oscillator strength of the lowest singlet excited state (f = 0.009 vs. f = 0.002 and f = 0.001, respectively).

Finally, a host material for SL-PhOLED should present an excellent thermal stability for vacuum deposition and device operating. Thermogravimetric analyses (TGA) and differential scanning calorimetry (DSC) provide very high decomposition (T_d = 408 and 407 °C) and glassy transition (T_g = 149 and 128 °C) temperatures for **SQA-2-FPOPh$_2$** and **SIA-2-FPOPh$_2$** respectively (Figures S1 and S2, Supporting Information). These values are in the same range than those of **SQPTZ-2-FPOPh$_2$**[26] and show that the QA unit is interesting for SL-PhOLED applications.

SQA-2-FPOPh$_2$ was finally incorporated as host in SL-PhOLEDs. The general SL-PhOLED architecture is ITO/PEDOT:PSS (40 nm)/EML: host + 18 wt.% FIr6 (100 nm)/LiF (1.2 nm)/Al (100 nm) with ITO/PEDOT:PSS as the anode and LiF/Al as the cathode. In order to obtain the highest performance, FIr6 doping rate has been optimized between 10 wt.% and 30 wt.%. Extracted characteristics (luminance, current efficiency, power efficiency, EQE, and threshold voltage V_{ON}) were compared to determine the optimal doping rate to be 18 wt.% (see Supporting Information). In these conditions, **SQA-2-FPOPh$_2$** based SL-PhOLED exhibits a maximal external quantum efficiency (EQE_{max}) of 10.2 % at 0.01 mA cm^{-2}, a maximal luminance (L_{max}) of 7234 cd m^{-2} at 80 mA cm^{-2} and a low V_{ON} of 3.1 V, **Figure 5**. Note that there is no contribution of the host in the electroluminescent (EL) spectrum, the devices exclusively exhibiting the blue emission of FIr6 (Figure 5, bottom right) with very similar CIE coordinates (see the emission spectrum of FIr6 thin-film dispersed in **SQA-2-FPOPh$_2$** in Figure S27, Supporting Information).

For comparison purpose, **SQPTZ-2-FPOPh$_2$** and **SIA-2-FPOPh$_2$** have been incorporated in the same device architecture with the same FIr6 doping rate to show the influence of the three electron-rich units. The performances appear to be very different for both molecules with moderate EQE_{max}, measured below 6%. It was particularly intriguing for **SQPTZ-2-FPOPh$_2$**, which is the most efficient material reported to date in a green SL-PhOLED.[26]

To interpret the different performances, photophysics and morphology of the EMLs were investigated as well as charge transport of host materials. The EMLs were exactly those used in the above-mentioned device. To get additional insights on excitons transfers and photophysical mechanisms, steady state and time resolved spectroscopy experiments of the three EML using either, **SQA-2-FPOPh$_2$**, **SQPTZ-2-FPOPh$_2$** or **SIA-2-FPOPh$_2$** doped with 18% of

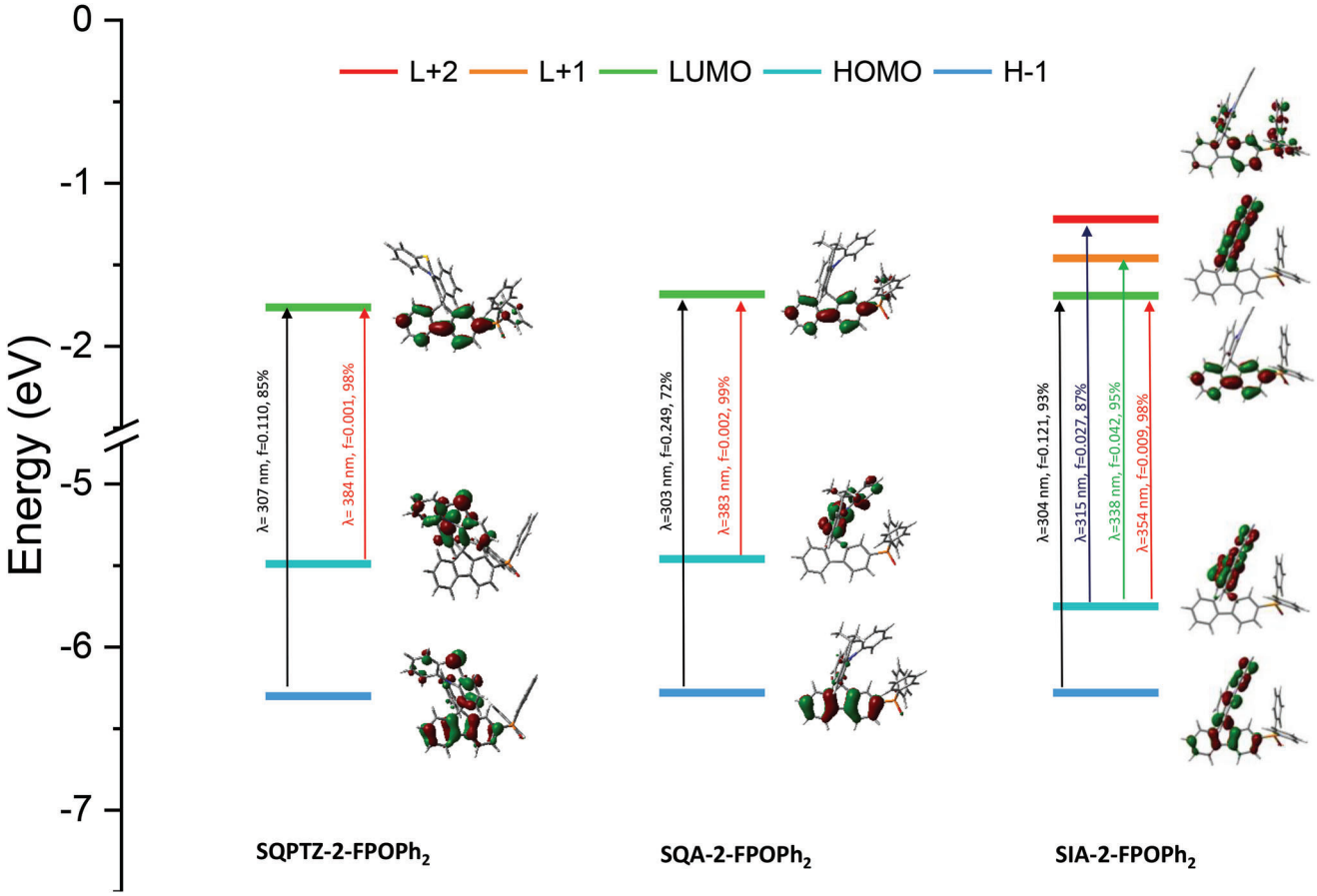

Figure 3. **SQPTZ-2-FPOPh$_2$** (Left), **SQA-2-FPOPh$_2$** (Middle) and **SIA-2-FPOPh$_2$** (Right). Representation of the energy levels and the main molecular orbitals involved in the electronic transitions obtained by TD-DFT, B3LYP/6–311+G(d,p), shown with an isovalue of 0.04 [ebohr^{-3}]$^{1/2}$. For clarity purposes, only the major contribution of each transition is shown (see Supporting Information for details).

FIr6 were performed. First of all, the three EMLs present photoluminescence spectra matching with their corresponding electroluminescence spectra (Figure S27, Supporting Information) showing the efficiency of the exciton's transfers. The lifetime decays of the different EMLs have been recorded at 1.0, 1.3, and 2.1 µs for **SQPTZ-2-FPOPh$_2$**, **SIA-2-FPOPh$_2$** and **SQA-2-FPOPh$_2$** respectively (see Figure S28, Supporting Information). Decreasing the triplet–triplet annihilation is an important feature to lead to a high device performance,[38–43] and it has been previously observed that the shortest lifetime in a series can lead to the highest performance.[26,38] Herein, the lifetime of the EML does not follow the PhOLED performance and does not seem to be the major parameter.

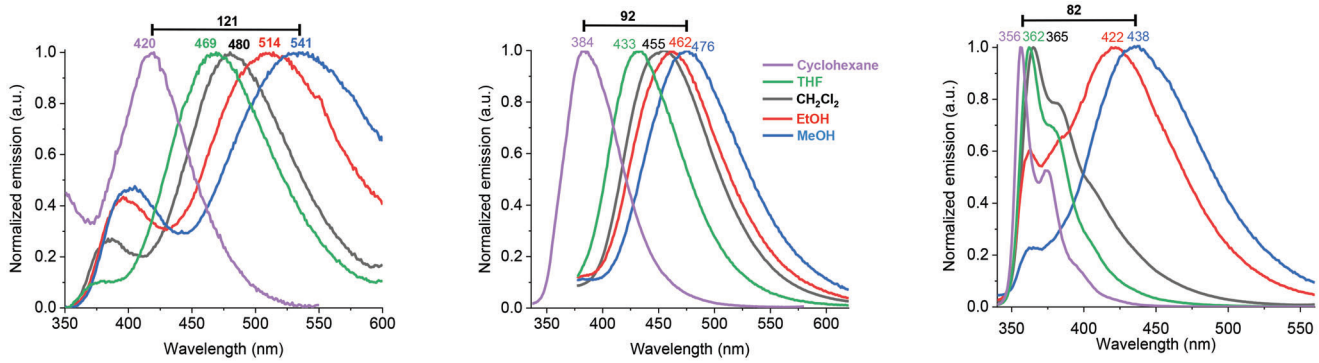

Figure 4. Emission spectra in various solvents **SQPTZ-2-FPOPh$_2$** (Left), **SQA-2-FPOPh$_2$** (Middle) and **SIA-2-FPOPh$_2$** (Right).

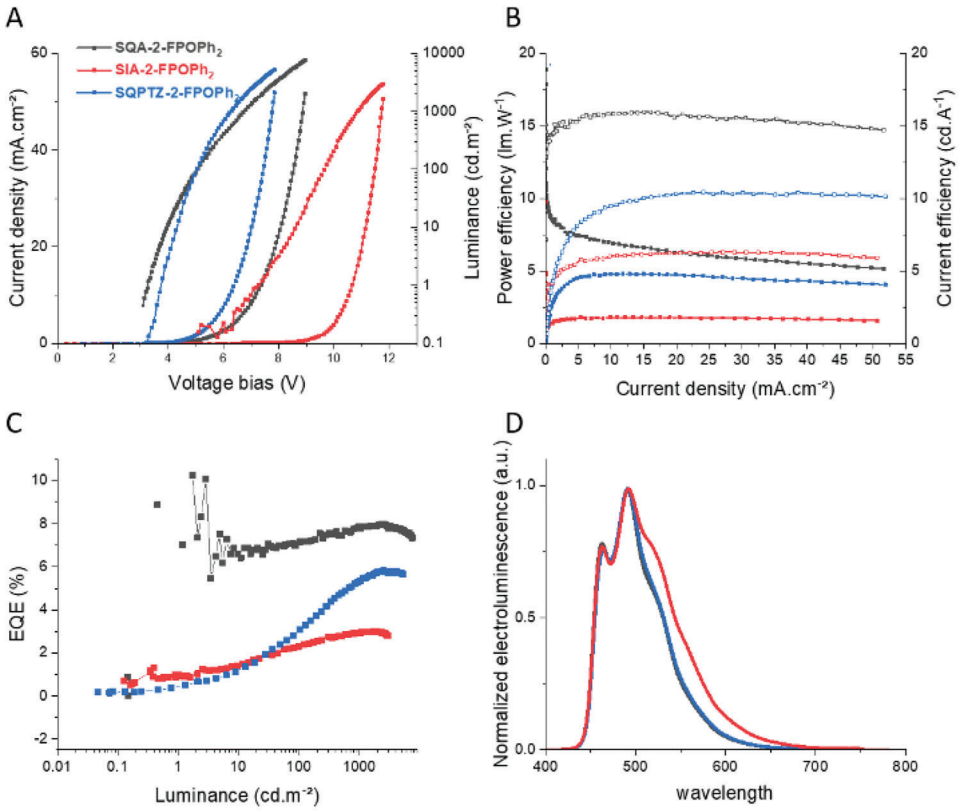

Figure 5. FIr6-based SL-PhOLED performances of **SQA-2-FPOPh$_2$** (black lines), **SIA-2-FPOPh$_2$** (red lines) and **SQPTZ-2-FPOPh$_2$** (blue lines). A) Current density and luminance as a function of voltage bias; B) power (■) and current (□) efficiencies as function of current density; C) Roll-off efficiency: EQE as function of luminance; D) Normalized electroluminescent spectra at 10 mA cm^{-2}.

In this field of simplified SL-PhOLEDs, the ability of the host material to carry holes and electrons as balanced as possible is an important property to optimise the formation of excitons preferably within the centre of the EML.[10] This is due to the absence, in such a device, of functional organic layers that usually insure the injection, the transport and the blocking of the charges in order to maximize the exciton formation. Incorporation of the host materials in hole-only and electron-only space charge limited current (SCLC) diodes to extract charge carriers mobilities have been performed (see Supporting Information for device architectures, fabrication processes and electrical characteristics). The hole (μ_h) and electron (μ_e) mobilities of **SQA-2-FPOPh$_2$** have been estimated at 7.25×10^{-5} and 1.35×10^{-7} cm^2 V^{-1} s^{-1} respectively. **SIA-2-FPOPh$_2$** / **SQPTZ-2-FPOPh$_2$** display μ_h of 1.45×10^{-2} / 5.10×10^{-8} and μ_e of 8.53×10^{-8} / 1.10×10^{-4} cm^2 V^{-1} s^{-1}. First, it is important to note that, despite very similar molecular structures, the mobilities are very different for both hole and electron ranging from ≈10^{-2} to 10^{-8} cm^2 V^{-1} s^{-1} for holes and from 10^{-4} to 10^{-8} cm^2 V^{-1} s^{-1} for electrons with ratios μ_h/μ_e of 537, 169, 988 and 0.0005 respectively. Thus, the highest hole mobility in the series, obtained for **SIA-2-FPOPh$_2$**, is particularly high (1.45×10^{-2} cm^2 V^{-1} s^{-1}) for a *spiro* compound but leads to the lowest SL-PhOLEDs performance. The same remark can be done for the electron mobility of **SQPTZ-2-FPOPh$_2$**. However, in SL-PhOLEDs, as there are no other functional layers to insure the transport, the charges balance is more important than the intrinsic values to determine the OLED performance. In the case of **SQA-2-FPOPh$_2$** and **SIA-2-FPOPh$_2$**, holes are transported ≈500 and 100 000 times quicker than electrons while in the case of **SQPTZ-2-FPOPh$_2$** electrons are ≈2000 times quicker than holes, reflecting well the different performances obtained in SL-PhOLEDs. The more balance the charge flow, the higher the SL-PhOLED performance. This shows the key role played by the charge transport in the efficiency of a SL-PhOLED.

Finally, as the morphology of the active layer is also known to have a great impact on the performance of an organic electronic device,[44] the roughness of the different EMLs were investigated by AFM studies, **Figure 6**. In order to well mimic the different samples, the exact architecture of the SL-PhOLEDs, i.e., ITO/PEDOT:PSS (40 nm)/EML (100 nm), was used.

The film surface of **SQA-2-FPOPh$_2$** based-EML presents a very low root mean surface roughness (R_q) of 1.12 nm, whereas **SQPTZ-2-FPOPh$_2$** and **SIA-2-FPOPh$_2$** have a roughness of 3.18 and 2.67 nm respectively. As thin film organization has a major impact on recombination between hole and electron due to the trapping of carriers induced by structural defects, **SQA-2-FPOPh$_2$** seems to promote the best structural organization. Thus, both charge transport and AFM studies correlate the highest performance measured for **SQA-2-FPOPh$_2$** versus to the two other analogues.

In order to confirm the high efficiency and the potential of **SQA-2-FPOPh$_2$** in simplified devices, incorporation in green

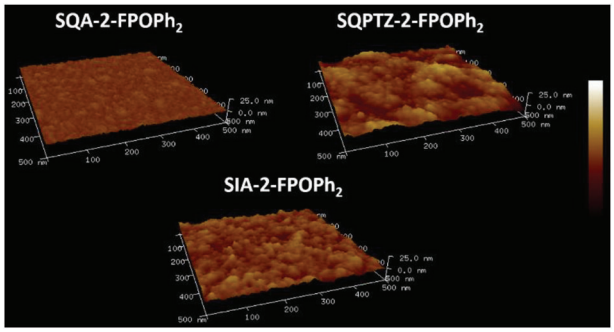

Figure 6. 1 2 D (500 × 500 nm^2) AFM images of (Top-left) **SQA-2-FPOPh$_2$** /18% Fir6, (Top-Right) **SQPTZ-2-FPOPh$_2$** /18% Fir6 and (Bottom) **SIA-2-FPOPh$_2$** /18% Fir6 (100 nm).

SL-PhOLEDs was also performed using Ir(ppy)$_2$acac as phosphor. Recently, **SQPTZ-2-FPOPh$_2$** has revealed its very high efficiency in green SL-PhOLEDs with an EQE$_{max}$ above 22% at 0.01 mA cm^{-2} and of 11.9% at 10 mA cm^{-2} (Ir(ppy)$_2$acac doping rate of 8%).[26] As far as we know, this performance is the highest reported to date for green SL-PhOLEDs. Herein, we remarkably note that **SQA-2-FPOPh$_2$** displays a similar maximum performance than **SQPTZ-2-FPOPh$_2$** at low current density with an EQE of 19.3% (CE of 56.9 vs. 67.1 cd A^{-1}, **Table 2**). At 10 mA cm^{-2} (Ir(ppy)$_2$acac doping rate of 10%), **SQA-2-FPOPh$_2$** even presents higher performance than **SQPTZ-2-FPOPh$_2$** (EQE of 13.8 vs. 12.5%, CE of 49.3 vs. 43.4 Cd A^{-1}, and PE of 19.8 vs. 25.4 lm W^{-1}, Table 1).

The performance of **SQA-2-FPOPh$_2$**-based devices was compared to benchmark devices fabricated with commonly used commercially available hosts for blue PhOLEDs, namely 1,3-bis(*N*-carbazolyl)benzene (mCP, HOMO/LUMO: −5.64/−2.19 eV, E$_T$ = 3.05 eV) and 3,3′-bis(*N*-carbazolyl)−1,1′-biphenyl (mCBP, HOMO/LUMO −6.0/−2.4 eV, E$_T$ = 2.8 eV).[45–47] The SL-PhOLED architecture of these benchmark devices is identical to that shown above. The origin of the different performance can then only be attributed to the host. For both compounds, the SL-PhOLEDs performance appear to be extremely low with EQE$_{max}$ of 1.4 (mCP) and 1.1% (mCBP) at 11 and 30 mA cm^{-2} respectively. V$_{ON}$ are very high, 6.9 and 7.4 V, and L$_{max}$ very low, 702 cd m^{-2} (at 60 mA cm^{-2}) and 572 cd m^{-2} (at 80 mA cm^{-2}) for mCP and mCBP respectively (see Figure S26 and Table S12, Supporting Information). As these materials are mainly "hole transporting", the origin of these low performance can only be ascribed to a poor charge balance within the EML, confirming how this parameter is important for high efficiency SL-PhOLEDs. The high performances obtained with **SQA-2-FPOPh$_2$** show the efficiency of the Donor-*spiro*-Acceptor design to fabricate high performance SL-PhOLEDs.

To go deeper in the understanding of this molecular strategy, we have finally fabricated ML-PhOLEDs using a known and efficient architecture.[48] ITO/PEDOT:PSS (40 nm)/ 1,1-bis[(di-4-tolylamino)phenyl]cyclohexane (TAPC) (45 nm)/ 4,4′,4″-tris-(carbazol-9-yl)-triphenylamine (TCTA) (8 nm)/ **SQA-2-FPOPh$_2$**:FIr6 (18 wt.%, 20 nm)/1,3,5-tris(6-(3-(pyridin-3-yl)phenyl)pyridin-2-yl)benzene (TmPyPB) (55 nm)/LiF (1.2 nm)/Al (100 nm). This **SQA-2-FPOPh$_2$**-based ML device exhibits an EQE$_{max}$ of 10.1% at 0.02 mA cm^{-2}, a V$_{ON}$ of 2.6 V and CE and PE of 23.9 cd A^{-1} and 26.8 lm W^{-1}(Figure S25 and Table S12, Supporting Information). The extracted performances for the SL architecture are in the same range than the one obtains for the ML architecture, showing thus the synergy between the host design and the simplified OLED architecture.

As the efficiency of **SQA-2-FPOPh$_2$** as host material for SL-PhOLED was high, it was finally interesting to test it in the challenging white-emitting SL-PhOLED. Indeed, the development of white SL-PhOLEDs, almost absent from literature,[49] involve blue emitting SL-PhOLEDs, Therefore, **SQA-2-FPOPh$_2$** has been used as host in a device using two EML: a blue (FIrpic) and a yellow (PO-01), **Figure 7**. The device structure is the following: ITO/PEDOT:PSS (40 nm)/Emissive layer 1 **SQA-2-POPh$_2$**:FIrpic 13% (50 nm)/Emissive layer 2 **SQA-2-POPh$_2$**:PO-01 2%/LiF (1.2 nm)/Al (100 nm). A very high EQE$_{max}$ above 24% (at 0.01 mA cm$^{-2)}$ was reached with CE /PE of 69.1 cd A^{-1}/57.2 lm W^{-1}. Even at 10 mA cm^{-2}, the EQE remains high (16.1%) showing the stability of the electroluminescence in such conditions. Despite the CIE coordinates was not perfectly in the white region (0.40;0.48), they remain close to warm light and these very high performances undoubtedly show the real potential of quinolinoacridine fragment to reach high performance single-layer devices with different phosphorescent emitters. These

Table 2. Devices data.

Host	P (%)	V$_{on}$ (V)	At 10 mA cm^{-2}				Max (at J (mA cm^{-2})				At 10 mA cm^{-2}
			EQE (%)	CE (cd A^{-1})	PE (lm W^{-1})	L (cd m^{-2})	EQE (%)	CE (cd A^{-1})	PE (lm W^{-1})	L (cd m^{-2})	CIE coordinates (x ; y)
FIr6											
SQA-2-FPOPh$_2$	18	3.1	7.9	15.8	6.9	1425	10.2 (0.01)	20.5 (0.01)	18.9 (0.01)	7234 (80)	0.17; 0.35
SIA-2-FPOPh$_2$	18	6.1	2.9	6.0	1.8	404	3.0 (27.1)	6.3 (27.1)	1.7 (27.1)	1973 (70)	0.21; 0.40
SQPTZ-2-FPOPh$_2$	18	3.3	5.3	9.5	4.8	917	5.8 (24.1)	10.4 (24.1)	4.6 (24.1)	4207 (80)	0.17; 0.36
Ir(ppy)$_2$acac											
SQA-2-FPOPh$_2$	10	2.5	13.8	49.3	19.8	4647	19.3 (0.01)	68.9 (0.01)	56.9 (0.01)	33280 (120)	0.33; 0.63
SIA-2-FPOPh$_2$	10	2.9	11.2	40.7	14.2	3422	12.9 (0.1)	48.1 (0.1)	30.2 (0.1)	28120 (130)	0.33; 0.63
SQPTZ-2-FPOPh$_2$	10	2.7	12.5	43.4	25.4	4430	19.3 (0.01)	71.6 (0.01)	67.1 (0.01)	50330 (190)	0.34 ; 0.63

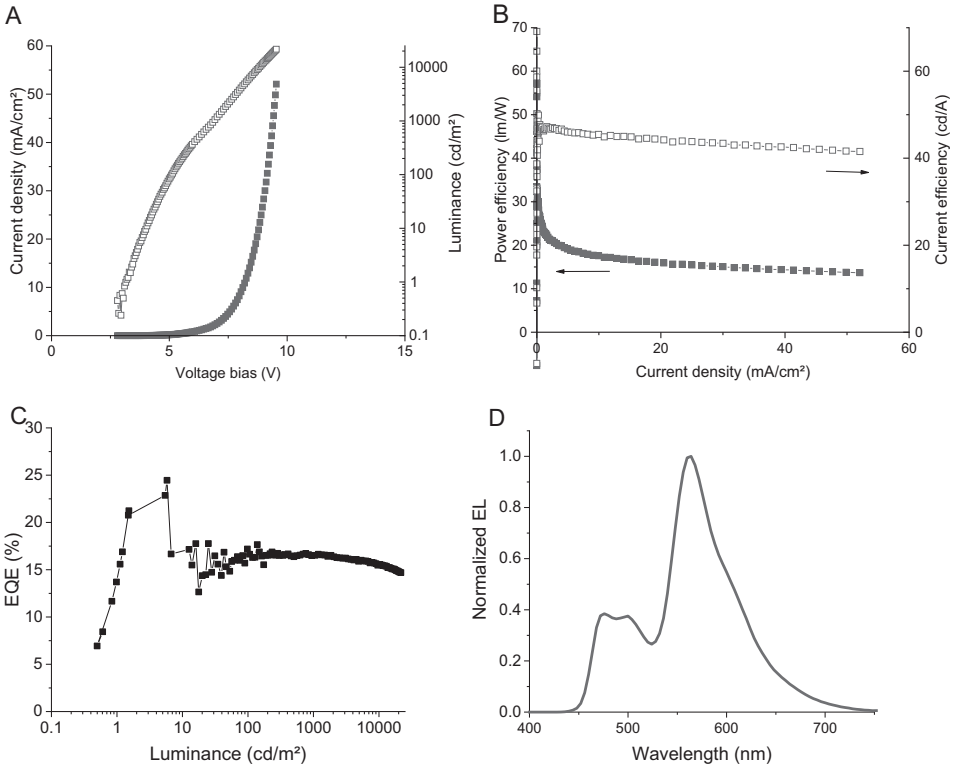

Figure 7. FIrPic/PO-01-**SQA-2-FPOPh$_2$** based device performances. A) Current density and luminance as a function of voltage bias; B) power and current efficiencies as function of current density; C) Roll-off efficiency: EQE as function of luminance; D) Normalized electroluminescent spectra at 10 mA cm^{-2}.

performances get close to those of recently reported ML-PhOLEDs.[50]

3. Conclusion

In summary, we propose herein a new host material, namely **SQA-2-FPOPh$_2$** for very high-performance SL-PhOLEDs. This molecule is constructed on the promising QA electron rich fragment. **SQA-2-FPOPh$_2$** gathers an adequate combination of photophysical, electronic, thermal, and morphological properties for high performance multi-coulour SL-PhOLEDs. The blue emitter used is FIr6, which has been very rarely used in the field of SL-PhOLEDs. For the first time, an EQE above 10% at 0.01 mA cm^{-2} is recorded (CE = 20.5 cd A^{-1}, PE = 18.9 lm W^{-1}, V_{on} = 3.1 V and L_{max} = 7234 cd m^{-2} at 80 mA cm^{-2}, CIE coordinates: 0.17;0.35 at 10 mA cm^{-2}). In green emitting SL-PhOLEDs, **SQA-2-FPOPh$_2$** displays a very high EQE, above 19% at 0.01 mA cm^{-2}, in the same range than the most efficient host (**SQPTZ-2-FPOPh$_2$**) reported to date for green SL-PhOLED. At 10 mA cm^{-2}, **SQA-2-FPOPh$_2$** even displays higher performance than its QPTZ analogue.

A comparison with structurally related host materials (**SQPTZ-2-FPOPh$_2$** and **SIA-2-FPOPh$_2$**) shed light on the different parameters (photophysical, charge transport and morphological) implied in the performance obtained. The balance of the charge transport appears as a key property to reach high performance in particular in the SL technology.

The performances of **SQA-2-FPOPh$_2$** are also significantly higher than those of well-known commercially available host matrices, mCBP and mCP. Comparison with a ML-PhOLED was also performed and revealed a similar efficiency clearly showing the great potential of such a design to simplify the PhOLED technology. Finally, this host was also used in a SL-PhOLED built on the superposition of a blue and a yellow EML. A very high EQE of 24.4% was reached with CIE coordinates of (0.40;0.48). This work shows the potential and the versatility of quinolinoacridine fragment to reach high performance multi-colour single-layer devices with different phosphorescent emitters. As blue emission and simplified PhOLEDs are both important for the future of this technology (and notably for simplified white SL-PhOLEDs), designing highly efficient organic semi-conductors and rationalizing their performance are important steps. We keep working in this direction.

Supporting Information

Supporting Information is available from the Wiley Online Library or from the author.

Acknowledgements

This work had been financially supported by the ANR (N 19-CE05-0024-*SpiroQuest* Project). C.B. and F.L. highly thank the ANR for PhD grant and postdoctoral fellowship respectively. The ADEME (Ecoelec Project, Dr Bruno Lafitte) was also warmly acknowledged for PhD grant (CB). This work received financial support under the EUR LUMOMAT project and the Investments for the Future program ANR-18-EURE-0012 (PhD grant DA). E.J. and C.P. thank the Université de Rennes for the allocation of a

Défi Scientique 2023-Recherche transdisciplinary interpoles. The authors also thank the CRMPO (Rennes) for mass analyses and GENCI (Project N°AD010814136) for computing time.

Conflict of Interest

The authors declare no conflict of interest.

Data Availability Statement

The data that support the findings of this study are available from the corresponding author upon reasonable request.

Keywords

charge transport, host materials, quinolinoacridine, single-layer phosphorescent OLED

Received: September 4, 2023
Published online: November 7, 2023

[1] C. Poriel, J. Rault-Berthelot, *Adv. Funct. Mat.* **2020**, *30*, 1910040.
[2] C. Poriel, J. Rault-Berthelot, Z.-Q. Jiang, *Mater. Chem. Front.* **2022**, *6*, 1246.
[3] A. Monkman, *ACS Appl. Mater. Interfaces* **2022**, *14*, 20463.
[4] J.-H. Lee, C.-H. Chen, P.-H. Lee, H.-Y. Lin, M.-k. Leung, T.-L. Chiu, C.-F. Lin, *J. Mater. Chem. C* **2019**, *7*, 5874.
[5] G. Hong, X. Gan, C. Leonhardt, Z. Zhang, J. Seibert, J. M. Busch, S. Bräse, *Adv. Mater.* **2021**, *33*, 2005630.
[6] Y. Wang, J. H. Yun, L. Wang, J. Y. Lee, *Adv. Funct. Mater.* **2020**, *31*, 2008332.
[7] Q. Zhang, B. Li, S. Huang, H. Nomura, H. Tanaka, C. Adachi, *Nat. Photonics* **2014**, *8*, 326.
[8] J. Lee, H.-F. Chen, T. Batagoda, C. Coburn, P. I. Djurovich, M. E. Thompson, S. R. Forrest, *Nat. Mater.* **2016**, *15*, 92.
[9] S. Madayanad Suresh, D. Hall, D. Beljonne, Y. Olivier, E. Zysman-Colman, *Adv. Funct. Mater.* **2020**, *30*, 1908677.
[10] C. Poriel, J. Rault-Berthelot, *Adv. Funct. Mater.* **2021**, *31*, 2010547.
[11] E. Baranoff, B. F. E. Curchod, *Dalton Trans.* **2015**, *44*, 8318.
[12] F. Lucas, C. Quinton, S. Fall, T. Heiser, D. Tondelier, B. Geffroy, N. Leclerc, J. Rault-Berthelot, C. Poriel, *J. Mater. Chem. C* **2020**, *8*, 16354.
[13] M. Idris, S. C. Kapper, A. C. Tadle, T. Batagoda, D. S. Muthiah Ravinson, O. Abimbola, P. I. Djurovich, J. Kim, C. Coburn, S. R. Forrest, M. E. Thompson, *Adv. Opt. Mater.* **2021**, *9*, 2001994.
[14] C. Jeong, C. Coburn, M. Idris, Y. Li, P. I. Djurovich, M. E. Thompson, S. R. Forrest, *Org. Electron.* **2019**, *64*, 15.
[15] M. Penconi, M. Cazzaniga, W. Panzeri, A. Mele, F. Cargnoni, D. Ceresoli, A. Bossi, *Chem. Mater.* **2019**, *31*, 2277.
[16] R. J. Holmes, B. W. D'Andrade, S. R. Forrest, X. Ren, J. Li, M. E. Thompson, *App. Phys. Lett.* **2003**, *83*, 3818.
[17] K. Gao, K. Liu, X.-L. Li, X. Cai, D. Chen, Z. Xu, Z. He, B. Li, Z. Qiao, D. Chen, Y. Cao, S.-J. Su, *J. Mater. Chem. C* **2017**, *5*, 10406.
[18] C. Wu, B. Wang, Y. Wang, J. Hu, J. Jiang, D. Ma, Q. Wang, *J. Mater. Chem. C* **2019**, *7*, 558.
[19] H.-H. Chang, W.-S. Tsai, C.-P. Chang, N.-P. Chen, K.-T. Wong, W.-Y. Hung, S.-W. Chen, *Org. Electron.* **2011**, *12*, 2025.
[20] F.-M. Hsu, L.-J. Chien, K.-T. Chen, Y.-Z. Li, S.-W. Liu, *Org. Electron.* **2014**, *15*, 3327.
[21] Z. Liu, M. G. Helander, Z. Wang, Z. Lu, *Org. Electron.* **2009**, *10*, 1146.
[22] Y. Yin, X. Wen, J. Yu, L. Zhang, W. Xie, *IEEE Photon. Technol. Lett.* **2013**, *25*, 2205.
[23] Y. Liu, L.-S. Cui, M.-F. Xu, X.-B. Shi, D.-Y. Zhou, Z.-K. Wang, Z.-Q. Jiang, L. S. Liao, *J. Mater. Chem. C* **2014**, *2*, 2488.
[24] A. Khan, X. Chen, S. Kumar, S.-Y. Yang, Y.-J. Yu, W. Luo, Z.-Q. Jiang, M.-K. Fung, L.-S. Liao, *J. Mater. Chem. C* **2020**, *8*, 12470.
[25] Y. K. Wang, C. C. Huang, H. Ye, C. Zhong, A. Khan, S. Y. Yang, M. K. Fung, Z. Q. Jiang, C. Adachi, L. S. Liao, *Adv. Opt. Mater.* **2019**, *8*, 1901150.
[26] F. Lucas, C. Brouillac, S. Fall, N. Zimmerman, D. Tondelier, B. Geffroy, N. Leclerc, T. Heiser, C. Lebreton, E. Jacques, C. Quinton, J. Rault-Berthelot, C. Poriel, *Chem. Mater.* **2022**, *34*, 8345.
[27] C. Brouillac, W.-S. Shen, J. Rault-Berthelot, O. Jeannin, C. Quinton, Z.-Q. Jiang, C. Poriel, *Mater. Chem. Front.* **2022**, *6*, 1803.
[28] F. Lucas, D. Tondelier, B. Geffroy, T. Heiser, O. A. Ibraikulov, C. Quinton, C. Brouillac, N. Leclerc, J. Rault-Berthelot, C. Poriel, *Mater. Chem. Front.* **2021**, *5*, 8066.
[29] C. Quinton, L. Sicard, O. Jeannin, N. Vanthuyne, C. Poriel, *Adv. Funct. Mat.* **2018**, *28*, 1803140.
[30] C. Poriel, J. Rault-Berthelot, S. Thiery, C. Quinton, O. Jeannin, U. Biapo, B. Geffroy, D. Tondelier, *Chemistry* **2016**, *22*, 17930.
[31] H. Jiang, J. Sun, *New J. Chem.* **2013**, *37*, 3161.
[32] S. Thiery, D. Tondelier, B. Geffroy, O. Jeannin, J. Rault-Berthelot, C. Poriel, *Chemistry* **2016**, *22*, 10136.
[33] Y.-X. Zhang, L. Ding, X.-Y. Liu, H. Chen, S.-J. Ji, L.-S. Liao, *Org. Electron.* **2015**, *20*, 112.
[34] J.-A. Seo, M. S. Gong, J. Y. Lee, *Org. Electron.* **2014**, *15*, 3773.
[35] P. Tourneur, F. Lucas, C. Brouillac, C. Quinton, R. Lazzaroni, Y. Olivier, P. Viville, C. Poriel, J. Cornil, *Adv Photonics Res* **2022**, *3*, 2200124.
[36] L. Sicard, C. Quinton, J.-D. Peltier, D. Tondelier, B. Geffroy, U. Biapo, R. Métivier, O. Jeannin, J. Rault-Berthelot, C. Poriel, *Chemistry* **2017**, *23*, 7719.
[37] L. J. Sicard, H.-C. Li, Q. Wang, X.-Y. Liu, O. Jeannin, J. Rault-Berthelot, L.-S. Liao, Z.-Q. Jiang, C. Poriel, *Angew. Chem., Int. Ed.* **2019**, *58*, 3848.
[38] Q. Wang, F. Lucas, C. Quinton, Y.-K. Qu, J. Rault-Berthelot, O. Jeannin, S.-Y. Yang, F.-C. Kong, S. Kumar, L.-S. Liao, C. Poriel, Z.-Q. Jiang, *Chem. Sci.* **2020**, *11*, 4887.
[39] A. Köhler, H. Bässler, *Mat. Sci. Eng. C- Reports* **2009**, *66*, 71.
[40] F. Steiner, J. Vogelsang, J. M. Lupton, *Phys. Rev. Lett.* **2014**, *112*, 137402.
[41] M. A. Baldo, C. Adachi, S. R. Forrest, *Phys. Rev. B* **2000**, *62*, 10967.
[42] Y.-K. Wang, Q. Sun, S.-F. Wu, Y. Yuan, Q. Li, Z.-Q. Jiang, M.-K. Fung, L.-S. Liao, *Adv. Funct. Mat.* **2016**, *26*, 7929.
[43] Q. Wang, Q.-S. Tian, Y.-L. Zhang, X. Tang, L.-S. Liao, *J. Mater. Chem. C* **2019**, *7*, 11329.
[44] M. Kumar, L. Pereira, *Nanomaterials* **2020**, *10*, 101.
[45] J. Ma, M. Idris, T. Y. Li, D. S. M. Ravinson, T. Fleetham, J. Kim, P. I. Djurovich, S. R. Forrest, M. E. Thompson, *Adv. Opt. Mater.* **2022**, *10*, 2101530.
[46] S. R. Forrest, *Phil. Trans. R. Soc.* **2015**, *373*, 20140320.
[47] U. Balijapalli, Y. T. Lee, B. S. Karunathilaka, G. Tumen-Ulzii, M. Auffray, Y. Tsuchiya, H. Nakanotani, C. Adachi, *Angew. Chem., Int. Ed.* **2021**, *133*, 19513.
[48] C. Brouillac, F. Lucas, D. Tondelier, J. Rault-Berthelot, C. Lebreton, E. Jacques, C. Quinton, C. Poriel, *Adv. Opt. Mater.* **2023**, *11*, 2202191.
[49] Y. Yin, X. Piao, Y. Li, Y. Wang, J. Liu, K. Xu, W. Xie, *Appl. Phys. Lett.* **2012**, *101*, 063306.
[50] F. C. Kong, Y. L. Zhang, C. Quinton, N. McIntosh, S. Y. Yang, J. Rault-Berthelot, F. Lucas, C. Brouillac, O. Jeannin, J. Cornil, Z. Q. Jiang, L. S. Liao, C. Poriel, *Angew Chem Int Ed Engl* **2022**, *61*, e202207204.